

www.acsami.org Research Article

Life Span of Slippery Lubricant Infused Surfaces

Muhammad Jahidul Hoque, Soumyadip Sett, Xiao Yan, Derrick Liu, Kazi Fazle Rabbi, Haoyun Qiu, Mansoor Qureshi, George Barac, Leslie Bolton, and Nenad Miljkovic*



Cite This: https://doi.org/10.1021/acsami.1c17010

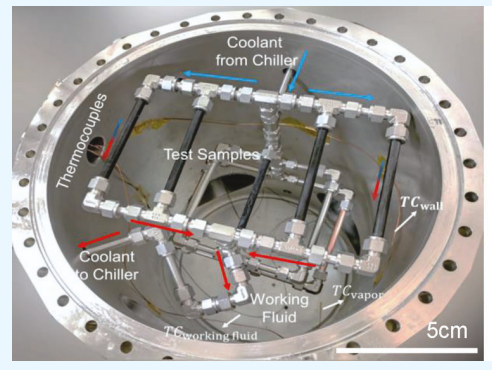


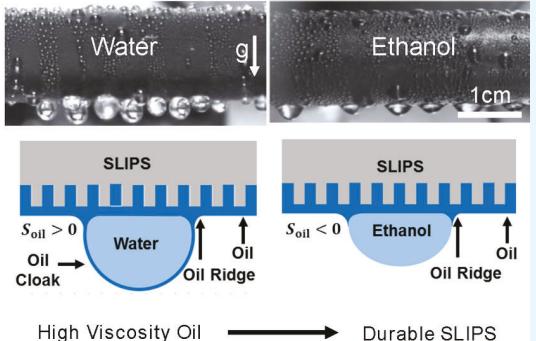
ACCESS

III Metrics & More

Article Recommendations

Supporting Information





ABSTRACT: Since their discovery a decade ago, slippery liquid infused porous surfaces (SLIPSs) or lubricant infused surfaces (LISs) have been demonstrated time and again to have immense potential for a plethora of applications. Of these, one of the most promising is enhancing the energy efficiency of both thermoelectric and organic Rankine cycle power generation via enhanced vapor condensation. However, utilization of SLIPSs in the energy sector remains limited due to the poor understanding of their life span. Here, we use controlled conditions to conduct multimonth steam and ethanol condensation tests on ultrascalable nanostructured copper oxide structured surfaces impregnated with mineral and fluorinated lubricants having differing viscosities (9.7 mPa·s < \mu < 5216 mPa·s) and chemical structures. Our study demonstrates that SLIPSs lose their hydrophobicity during steam condensation after 1 month due to condensate cloaking. However, these same SLIPSs maintain nonwetting after 5 months of ethanol condensation due to the absence of cloaking. Surfaces impregnated with higher viscosity oil (5216 mPa·s) increase the life span to more than 8 months of continuous ethanol condensation. Vapor shear tests revealed that SLIPSs do not undergo oil depletion during exposure to 10 m/s gas flows, critical to condenser implementation where single-phase superheated vapor impingement is prevalent. Furthermore, higher viscosity SLIPSs are shown to maintain good stability after exposure to 200 °C air. A subset of the durable SLIPSs did not show change in slipperiness after submerging in stagnant water and ethanol for up to 2 weeks, critical to condenser implementation where single-phase condensate immersion is prevalent. Our work not only demonstrates design methods and longevity statistics for slippery nanoengineered surfaces undergoing long-term dropwise condensation of steam and ethanol but also develops the fundamental design guidelines for creating durable slippery liquid infused surfaces.

KEYWORDS: SLIPS, LIS, ethanol, steam, durable, dropwise, condensation, low surface tension

Biomimicry is a practice that translates nature-inspired design into sustainable solutions. Taking inspiration from the lotus leaf, synthetic highly water-repellent superhydrophobic surfaces have been developed and extensively studied for application to a wide range of technologies. Traditional superhydrophobic surfaces rely on creating air infused microand nanostructures to minimize the contact between water and the substrate. Although promising, widespread use of superhydrophobic surfaces is restricted due to a lack of long-term durability, surface flooding at high humidity or droplet impact velocity, droplet contact line pinning due to defects, and loss of water repellency at elevated pressures and temperatures. The furthermore, superhydrophobic surfaces fail to repel low surface tension liquids, with adsorption

of organic contaminants such as proteins, cells, or bacteria compromising repellency. $^{17-19}\,$

Although complex re-entrant geometries can achieve repellency of deposited low surface tension liquids, ^{3,20,21} they fail during condensation, where the presence of random nucleation sites leads to flooding and film formation. ^{10,22} Usage of low surface tension liquid has grown substantially in

Received: September 3, 2021 Accepted: December 23, 2021



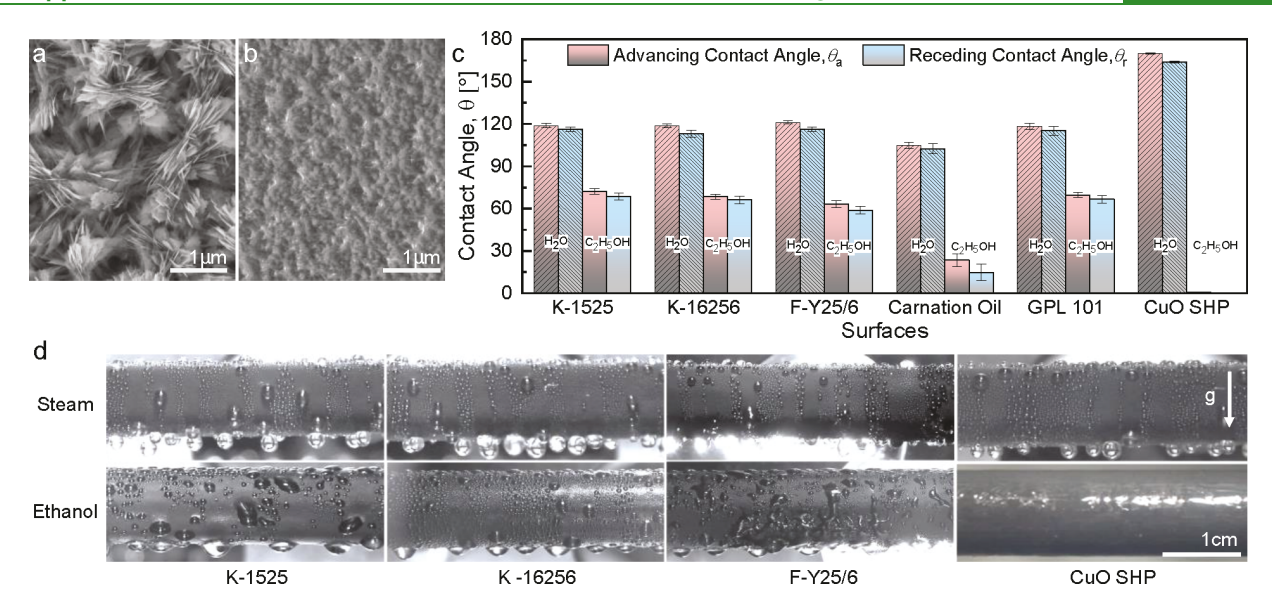


Figure 1. Surface wettability characterization of different SLIPS. Scaning electron microscopy (SEM) images of a (a) superhydrophobic CuO surface and (b) Krytox 1525 infused CuO SLIPS. (c) Goniometric contact angle measurements of DI water and ethanol droplets on the studied samples. (d) Optical images of external condensation of steam and ethanol vapor on different SLIPS and the superhydrophobic CuO surface. SLIPSs infused with Krytox 1525, Krytox 16256, and Fomblin are named K-1525, K-16256, and F-Y25/6, respectively. Sueprhydrophobic CuO is termed CuO SHP. The contact angle of ethanol on the CuO SHP surface is difficult to measure and is not reported as ethanol completely wets the

recent years due to their implementation as alternative energy sources, biofuels, and refrigeration applications. 23-28 Hence, the development of durable surfaces that are repellant to low surface tension fluids is needed.

Inspired by the Nepenthes pitcher plant, a new class of surface called the slippery liquid infused porous surface (SLIPS) has been proposed.²⁹ Here, a textured solid is infiltrated with a physically and chemically confined immiscible lubricant to create a smooth liquid over layer capable of addressing the challenges associated with maintaining stable air pockets. SLIPS are omniphobic, exhibit essentially no contact line pinning, are stable at high pressures, 29,30 and display selfhealing to mechanical damage.²⁹ Moreover, SLIPS have ultralow contact angle hysteresis and show rapid droplet shedding of low surface tension liquids because of the presence of a chemically homogeneous and atomically smooth interface for both deposited and condensing liquid droplets.31-33 Because of their superior repellant properties to a variety of liquids, SLIPS have been demonstrated to promote stable dropwise condensation of low surface tension organic vapors and enhanced dropwise condensation heat transfer. 34-37 Dropwise condensation of ethanol and hexane on SLIPS in pure vapor environments shows a 200% heat transfer enhancement when compared to smooth hydrophobic or hydrophilic metal surfaces during continual 7 h tests. 38,39 However, the majority of technologies promising for SLIPS implementation have longevity time scales at a minimum of months (consumer products), with the majority having operating lifetime requirements of multiple years (industrial equipment).

The life span of SLIPS is of crucial importance for both system performance and economic considerations. A lack of fundamental understanding of condensation-induced degradation mechanisms has held back the successful development and demonstration of surfaces capable of achieving stable dropwise condensation. One of the largest barriers to success is the long

experimental time scale required to quantify life span. A limited number of studies have focused on conducting long-term condensation durability tests on functional surfaces. 40-46 To the best of our knowledge, no study has quantified the longterm (multimonth) condensation durability of SLIPS. The majority of past work has focused on short-term robustness quantification for icing/frosting, biofouling, corrosion, and aging.⁴⁷⁻⁵⁴ Here, we conduct rigorous multimonth durability studies of SLIPS during relevant steam and ethanol condenser conditions. We focus our degradation conditions to condensers given the clear and promising use case for SLIPS. Specifically, we design and test a holistic array of durability conditions which aim to emulate realistic scenarios that SLIPS would encounter if implemented within large scale shell and tube condensers. These include single-phase vapor shear (condenser inlet), elevated temperature exposure to air (manufacturing), long-term condensation tests (condensation), and immersion for prolonged periods within water and ethanol (condenser outlet). We use rationally designed ultrascalable nanostructured copper oxide (CuO) SLIPS impregnated with vacuum grade lubricants covering a wide range of viscosities (9.7-5216 mPa·s). Our work forms the basis for science-based fabrication of durable SLIPS.

RESULTS

Fabrication and Wettability of SLIPS. To fabricate the SLIPS, we used copper (Cu) as a base substrate. Commercially available Cu tubes with outer diameters $d_{\rm OD}$ = 9.52 mm, inner diameters $d_{\rm ID}$ = 8.73 mm, and lengths L = 108 mm were used as the test samples. The fabrication process starts with cleaning the uncapped Cu tube by dipping it for 15 min in acetone, ethanol, isopropanol, and deionized (DI) water, in succession, followed by rinsing with DI water. The tubes were then dipped into a 2.0 M hydrochloric acid solution for 2 min to remove the native oxide layer on the surface, then rinsed multiple times with DI water, and dried with clean nitrogen gas stream.

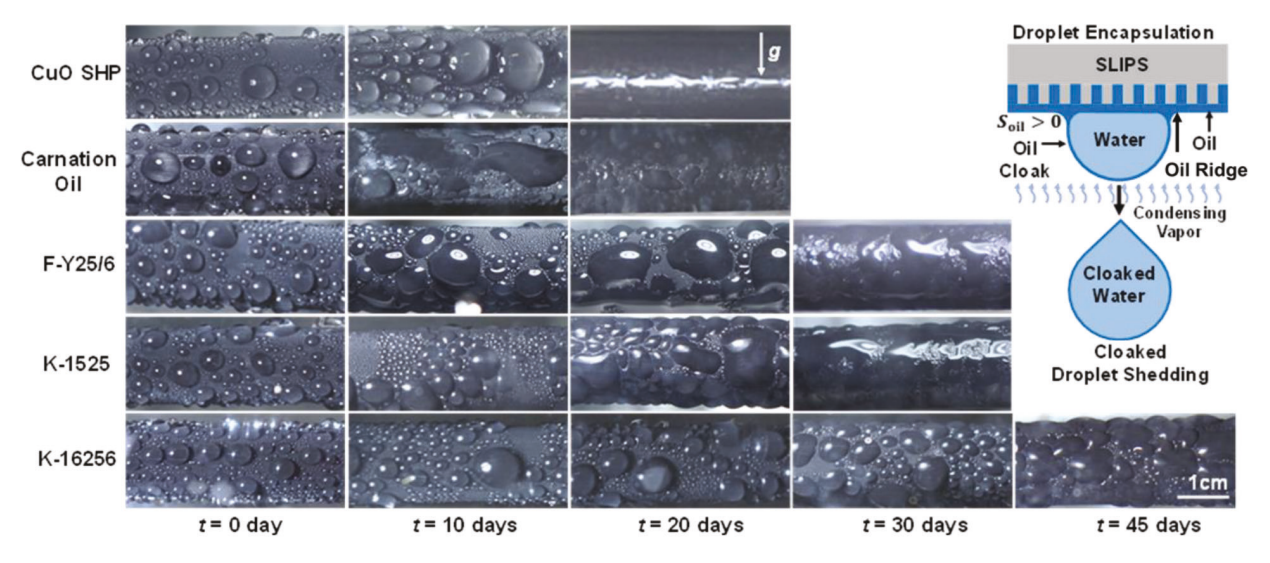


Figure 2. Steam condensation durability. Time-lapse optical images of the samples during steady steam condensation. The superhydrophobic (CuO SHP) tube surface and the carnation oil infused SLIPS sample degraded after 10 days, with both surfaces transitioning to filmwise condensation within 20 days after test initiation. The F-Y25/6 and K-1525 infused SLIPS performs well for ~21 days, with transition to filmwise condensation within 28 days. The highly viscous K-16256 infused SLIPS did not show filmwise condensation after 45 days of continuous steam condensation. Schematics (not to scale) on right: oil with positive spreading coefficient forms an oil cloak around the condensate; cloaked condensate shedding increases the oil depletion rate, resulting in reduction of the slippery life span.

Afterward, dense blade-like nanostructured CuO surfaces were formed by immersing the capped cleaned tubes into a hot (90 ± 5 °C) alkaline bath of NaClO₂, NaOH, Na₃PO₄·12H₂O, and DI water (3.75:5:10:100 wt %).55 Surfaces were then functionalized by using atmospheric pressure chemical vapor deposition (CVD) of a fluorinated silane (heptadecafluorodecyltrimethoxysilane, HTMS, Gelest, CAS #83048-65-1).5 Lubricants of choice were next impregnated into the functionalized superhydrophobic CuO samples by dipping them into the lubricant. After dipping the samples in the lubricant for 10 min, drainage of the excess lubricant from the surface was ensured by leaving the tubes in a vertical position for 24 h in ambient conditions followed by drying in a clean nitrogen stream. Gravitational drainage of excess oil from the surfaces for 24 h ensures the presence of lubricant only within the nanostructures, which was shown to be independent of the oil viscosity.³⁹ From a theoretical perspective, we estimate the amount of oil retained in the CuO structure by considering that, irrespective of the oil viscosity, the lubricant fills the CuO microstructures (structure height $h \approx 2 \mu m$, solid fraction $\varphi \approx$ 0.023). Thus, at initiation of the experiments, the SLIPSs have $\approx\!\!2~mL/m^2~(\approx\!\!3.8~g/m^2)$ of lubricant per unit condenser surface area. 57

Here we used Krytox 16256 (5216 mPa·s at 20 °C), Fomblin 25/6 (524 mPa·s at 20 °C), Krytox 1525 (496 mPa·s at 20 °C), Carnation oil (9.7 mPa·s at 20 °C), and GPL 101 (14.7 mPa·s at 20 °C) as the infusing lubricants. These lubricants were rationally selected to cover a wide range of vapor pressures at room temperature (4.0 \times 10 $^{-15}$ –1.3 \times 10 $^{-8}$ kPa), viscosity (9.7–5216 mPa·s), and to some extent surface tension (18–28 mN/m). Details of the fabrication process and physical properties of the infused oils are included in section S1 and Table S1 of the Supporting Information.

Fluorinated and mineral oils were selected as lubricants due to their immiscibility with water and ethanol as well as their differing spreading behavior at the condensate/oil interface (Table S1).⁵⁸ Figures 1a and 1b show scanning electron micrographs (SEM) of a functionalized CuO and lubricant

(Krytox 1525) infused CuO SLIPS, respectively. The contact angle of water and ethanol on each sample was measured by using microgoniometry (MCA-3, Kyowa Interface Science), where liquid droplets (100 nL) were dynamically grown to measure the apparent advancing contact angles. The microgoniometer droplet dispenser was then turned off, and the deposited droplets were allowed to continuously evaporate to obtain the apparent receding contact angle. ^{59–61} All SLIPS surfaces showed <5° contact angle hysteresis (Figure 1c). Ethanol droplets made a thin film after impacting the superhydrophobic CuO surface, making it difficult to measure the contact angle (Figure 1c). Similarly, condensation of ethanol on the superhydrophobic CuO surface resulted in liquid film formation (Figure 1d). As expected, ³⁹ all SLIPS showed dropwise condensation during short-term (<1 day) condensation experiments.

Long-Term Durability during Steam Condensation. To conduct condensation durability studies on SLIPS relevant to thermoelectric power generation applications, we exposed the samples to continual steam condensation. Four SLIPSs infused with carnation oil, Fomblin (F-Y25/6), Krytox 1525 (K-1525), Krytox 16256 (K-16256), and one superhydrophobic (SHP) CuO sample were placed in the chamber. Condensation experiments and visualization were continuously conducted. The long-term condensation durability experiments were conducted in a customized chamber maintaining a pressure of ~5 kPa. To maintain the same level of pressure throughout the long-term durability test, the condensation rig had to be shut down once per month to pump down the chamber to the desired pressure level to remove noncondensable gases. This was done due to air leaking into the chamber at a slow rate from the atmosphere-to-saturated vapor (subatmospheric pressure) pressure difference. During shutdown, the chamber was not opened, and only the cooling water flowing through the tubes was arrested. During shutdown, the chamber was vacuumed through a valve feedthrough to remove noncondensable gases, with shutdown lasting no more than 3 h per month. For the remaining time,

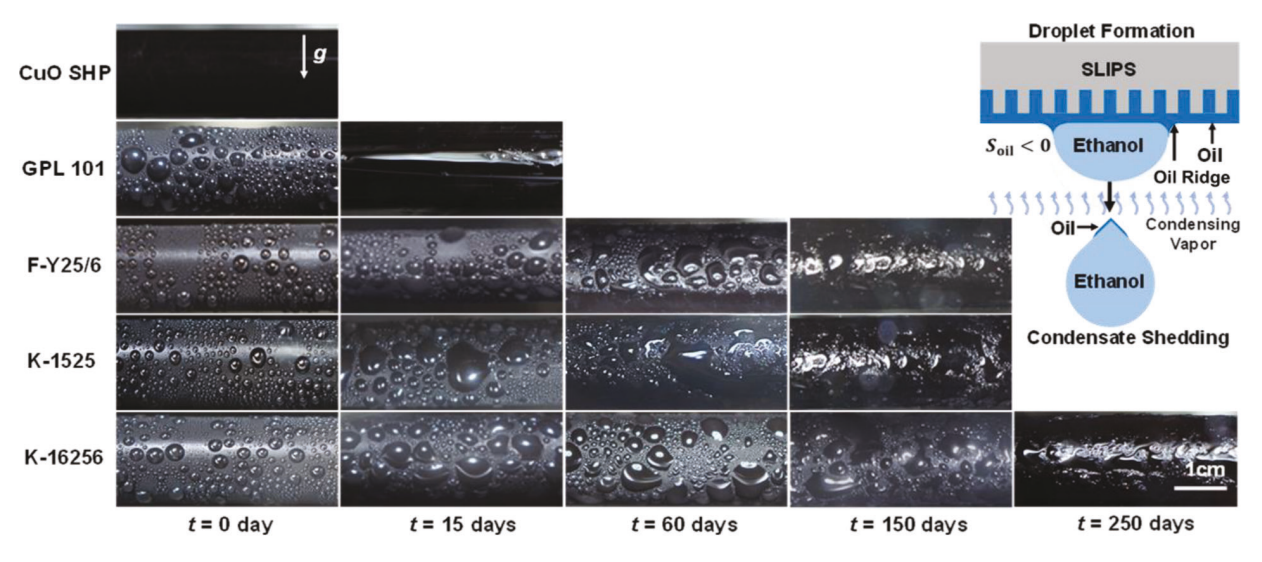


Figure 3. Ethanol condensation durability. Time-lapse optical images of the samples during steady ethanol condensation. The superhydrophobic (CuO SHP) tube surface shows filmwise condensation immediately after starting condensation (t = 0). The GPL-101 infused SLIPS degrades in 14 days, showing filmwise transition. The F-Y25/6, and K-1525 infused SLIPSs degraded at 5 months of continual ethanol condensation exposure, with the highly viscous K-16256 infused SLIPS degrading after 8 months. Unlike steam condensation, SLIPS samples exposed to ethanol condensation show stable filmwise—dropwise hybrid condensation before eventual transition to filmwise. Schematics (not to scale) on right: oil with negative spreading coefficient does not cloak the condensate; however, because of condensate shear, oil depletes at a very slow rate, delaying the oil depletion and hence increasing the life span of the SLIPS. The oil layer on the trailing edge of the shedding droplet does not imply the actual mechanism of oil depletion.

continual 24 h a day condensation occurred in the chamber. Details of the durability test setup and testing procedures are discussed in the Methods section.

Condensation of steam on the surfaces was visualized over long periods of time to evaluate surface degradation (Figure 2). For steam condensation, degradation or loss of hydrophobicity indicates that the DI water apparent advancing droplet contact angle decreases below 90° along with significant reduction of the receding contact angle. As a result, the contact angle hysteresis increases when compared to the freshly made sample. Visualization of the condensation transition from regular spherical shaped droplets (dropwise) to a surface flooded with irregular shaped droplets or thin condensate films provided a qualitative measure of surface degradation. The superhydrophobic CuO surface and carnation oil infused SLIPS degraded after 10 days of exposure to steam condensation, with both surfaces flooding within a 3-week period of initiating steady condensation (Figure 2).

In contrast, the F-Y25/6 and K-1525 infused SLIPS showed good shedding behavior for up to 1 month of steady-state steam condensation. Among all samples, K-16256 infused SLIPS showed no sign of degradation after 45 days of exposure to steam condensation. The viscosity and spreading coefficient of the impregnated oils play a vital role on the long-term durability of SLIPS during condensation. Variation in the longevity among the different SLIPS stems from the difference in oil ridge formation, cloaking phenomena (right schematic in Figures 2 and 3), and contrast in the rate of oil depletion with shedding condensate droplets resulting from the viscosity differences of the infused oils. Condensate encapsulation or cloaking of the condensate droplets by the infused oil was observed when the spreading coefficient of the oil on the condensate (S_{oil}) is positive $(S_{oil} > 0)$. The spreading coefficient $S_{\rm oil}$ is defined as $S_{\rm oil} = \gamma_{\rm droplet} - \gamma_{\rm oil} - \gamma_{\rm oil-droplet}$ where $\gamma_{\rm droplet}$ $\gamma_{\rm oil}$ and $\gamma_{\rm oil-droplet}$ represent the surface tension of the condensing droplet, lubricant oil, and interfacial tension

between the droplet and oil, respectively. Cloaked condensate sheds from the surface and over time reduces the slipperiness of the surfaces by depleting the infused oil layer (right schematic in Figure 2). Carnation oil has a negative spreading coefficient ($S_{\text{carnation}} = -6.6 < 0$), which prevents cloaking. However, both K-1525 and K-16256 have positive spreading coefficients ($S_{Krytox} = 2.7 > 0$). Hence, the oil can spread and encapsulate the condensed water droplet.⁵⁸ Even though K-16256 has a positive spreading coefficient, the shedding of the cloaked droplets from the K-16256 infused SLIPS had the lowest oil depletion rate due to the highest viscosity (μ = 5216 mPa·s) among the tested samples. Because of its negative spreading coefficient, carnation oil hinders cloaking. However, the surface loses its slipperiness in a very short period of time because the infused carnation oil has a very low viscosity (μ = 9.7 mPa·s) and is removed via shear-induced drainage.

Our results show that even in the presence of droplet cloaking, the viscosity of the infused oil plays a more dominant role on the life span of SLIPS during condensation. Past studies have shown that a major source of oil depletion happens during oil ridge formation near the base of the departing droplet. 65,66 To evaluate the effects of oil viscosity variation on the droplet wetting ridge-driven oil depletion, we performed a scaling analysis to compare with cloak-layer-driven oil depletion. The volume of a condensate droplet (V_{droplet}) with an apparent advancing contact angle, θ , and radius, R, can be expressed as $^{67} V_{\text{droplet}} = (\pi/3)[(1 - \cos \theta)^2(2 + \cos \theta)R^3].$ The volume of a cloak layer $(V_{\rm cloak\,layer})$ on the condensate droplet can be calculated from the difference between original droplet size and size increment due to a cloak layer with a thickness t. Thus, $V_{\text{cloak layer}} = (\pi/3)[(1 - \cos \theta)^2(2 + \cos \theta)]$ $[\theta]$ $[(R+t)^3-R^3]$. Assuming, a 2 mm diameter condensate droplet with a contact angle of 120° having a 10 nm cloak layer, the volume of the cloak layer becomes $V_{\rm cloak\,layer}$ = 1.06 \times 10⁻¹³ m³. The volume of the oil ridge around a condensate droplet can be expressed as 66 $V_{\text{ridge}} = R_{\text{b}} h_{\text{i}}^2 / \mu_1 C a^{4/3}$, where R_{b}

Table 1. Characterization of Samples after Steam and Ethanol Condensation Durability Tests^a

					lifetime [days]	
surface	infused oil	μ [mPa·s]	$\Delta heta_{ ext{water}} \ [ext{deg}]$	$\Delta heta_{ m ethanol} \ [m deg]$	steam	ethanol
CuO-HTMS	N/A	N/A	4.1	N/A	20	1
CuO-HTMS	carnation oil	9.7	2.8 ± 1.1	8.7 ± 1.3	20	N/A
	GPL101	14.7	3.2 ± 1	2.8 ± 1.2	N/A	10
	Fomblin	524	2.9 ± 2.7	2.2 ± 3.1	30	150
	Krytox 1525	496	2.7 ± 2.6	2.3 ± 2.9	30	150
	Krytox 16256	5216	3.2 ± 2.9	2.8 ± 3.2	45	250

 $^{^{}a}$ The measured $\Delta heta_{ ext{water}}$ and $\Delta heta_{ ext{ethanol}}$ characterize the water droplet and ethanol droplet contact angle hysteresis prior to conducting condensation experiments. Lifetime is defined as the condensation exposure time required to transition the condensation mode from dropwise or hybrid dropwise-filmwise to classical filmwise condensation.

is the base radius of the droplet, h_i is the initial lubricant film thickness, $\mu_1 \sim 0.5$ is the limiting size of the wetting ridge for a given set of experimental conditions, ⁶⁶ and $Ca = \eta U/\gamma$ is the capillary number. Here η is the oil viscosity, γ is the surface tension of the oil, and U is the droplet shedding velocity. For a departing condensate droplet ($R_b = 2 \text{ mm}$) shedding at 2 mm/ s on K-16256 (η = 5216 mPa·s; γ = 19 mN/m) and K-1525 (η = 496 mPa·s; γ = 19 mN/m) infused SLIPS with an initial oil layer thickness, $h_{\rm i}=2~\mu{\rm m}$, the oil ridge volumes are $V_{\rm ridge,K-16256}=1.78\times10^{-14}~{\rm m}^3$ and $V_{\rm ridge,K-1525}=4.09\times10^{-13}~{\rm m}^3$. Our analysis shows that for SLIPS with high viscosity oil (K-16256) the cloak-layer-driven oil depletion dominates ridge induced oil depletion ($V_{\text{cloak layer}} = 1.06 \times 10^{-13} \text{ m}^3 > V_{\text{ridge,K-16256}} = 1.78$ \times 10⁻¹⁴ m³). However, this ratio of depletion rates becomes smaller for lower viscosity oils ($V_{\text{ridge,K-1525}} = 4.09 \times 10^{-13} \text{ m}^3 \sim$ $V_{\text{cloak laver}}$). Because of having the same order of magnitude oil viscosities, both K-1525 and F-Y25/6 show similar behavior.

The scaling analysis appears to signify that the volume of the cloak layer is independent of the oil viscosity while the oil ridge volume is viscosity dependent. The life span predicted by using the scaling analysis shows large divergence from the experimental observations (see section S4 of the Supporting Information). The differences between theory and experiment are attributed to multiple factors. The scaling analysis was developed for and assumes that the cloak layer thickness is uniform irrespective of oil viscosity. However, in reality, the cloak layer is spatially and temporally nonuniform when compared to the lubricant underneath and behind a moving droplet. 65,66 Furthermore, the cloak layer formation time scale is viscosity dependent. 63,65 In the oil ridge volume analysis, the droplet size and shedding velocity were assumed to be similar for different SLIPSs. Oil depletion due to oil ridge formation is a function of the departure velocity and oil viscosity. As the viscosity of the infused oil increases, the departure velocity decreases.⁶⁵ Oil depletion from the surface is governed by a dynamic balance between droplet cloaking, oil ridge formation, and droplet shear. Moreover, the analysis is not developed to capture the possible change in interfacial phenomena due to the gradual reduction of oil volume on SLIPSs, which may lead to changes in the cloak layer and oil ridge formation time scale as well as variation in dimensions. Additional details regarding the scaling analysis model and life span predictions can be found in section S4 of the Supporting Information.

Long-Term Durability during Ethanol Condensation. To conduct condensation durability studies on SLIPS relevant to organic Rankine cycle and petrochemical separations condenser applications, we exposed the samples to continual ethanol vapor condensation conditions. In addition to the high viscosity SLIPS (F-Y25/6, K-1525, and K-16256), we also

tested a SLIPS infused with a very low viscosity oil (GPL-101, 14.7 mPa·s). Although the carnation oil has a negative spreading coefficient in both water and ethanol ($S_{carnation,water}$ = -6.6; $S_{\text{carnation,ethanol}} = -10$), it was not included in the ethanol condensation tests due to its demonstrated poor durability during steam condensation (Figure 2). Similarly, GPL-101 was not used during steam condensation due to its positive spreading coefficient ($S_{GPL101,water} = 2.9 > 0$) and low viscosity ($\mu = 14.7 \text{ mPa·s}$). For ethanol condensation, we included GPL-101 because of its unique spreading coefficient with ethanol condensate ($S_{GPL101,ethanol} = 0$, Table S1).

Experiments revealed that the low surface tension ethanol condensate (24.8 mN/m) forms a film on the superhydrophobic (SHP) surface immediately after condensation initiation (Figure 3). As expected, because of its low viscosity, the GPL-101 infused SLIPS degraded within 14 days of continuous exposure to ethanol condensation. For ethanol, because the apparent advancing contact angle was already below 90° on the fresh surfaces, the indication of loss of ethanol repellency was measured by the increase in contact angle hysteresis stemming from the substantial decrease in the receding contact angle, which leads to irregular droplet shape (or film) formation during condensation.⁶⁸ The Krytox oil infused SLIPS (K-1525 and K-16256) and Fomblin (F-Y25/6) have negative spreading coefficients with ethanol condensate (Table S1), resulting in the absence of cloaking and delayed oil depletion. By preventing cloaking, high viscosity SLIPSs show longer durability to ethanol condensation when compared to steam condensation (Figure 3 and Table 1). Because of the negative spreading coefficient, the condensates are not cloaked. Furthermore, evaporation of the infused oil is negligible as the volatility is low at ambient temperatures. Hence, oil mainly depletes due to oil ridge formation and condensate shear beneath shedding droplets (right schematic in Figure 3). As shown in Figure 3, compared to steam condensation, SLIPS infused with high viscosity oils (K-1525, K-16256, and F-Y25/ 6) showed continuous ethanol condensate shedding for more than 5 months of continual testing. In agreement with the steam condensation experiments, the K-16256 infused SLIPS had the greatest longevity, demonstrating stable dropwise condensation for more than 8 months (250 days) of continual ethanol condensation.

Condensate droplet dynamics of ethanol differ from water due to two different reasons. The first is that ethanol condensate and water have different surface tensions. The second is due to oil layer depletion from the underlying structure and resulting exposure of the underlying structure. The latter acts to decrease the lubricant-condensate interface area and increase the structure condensate interfacial area,

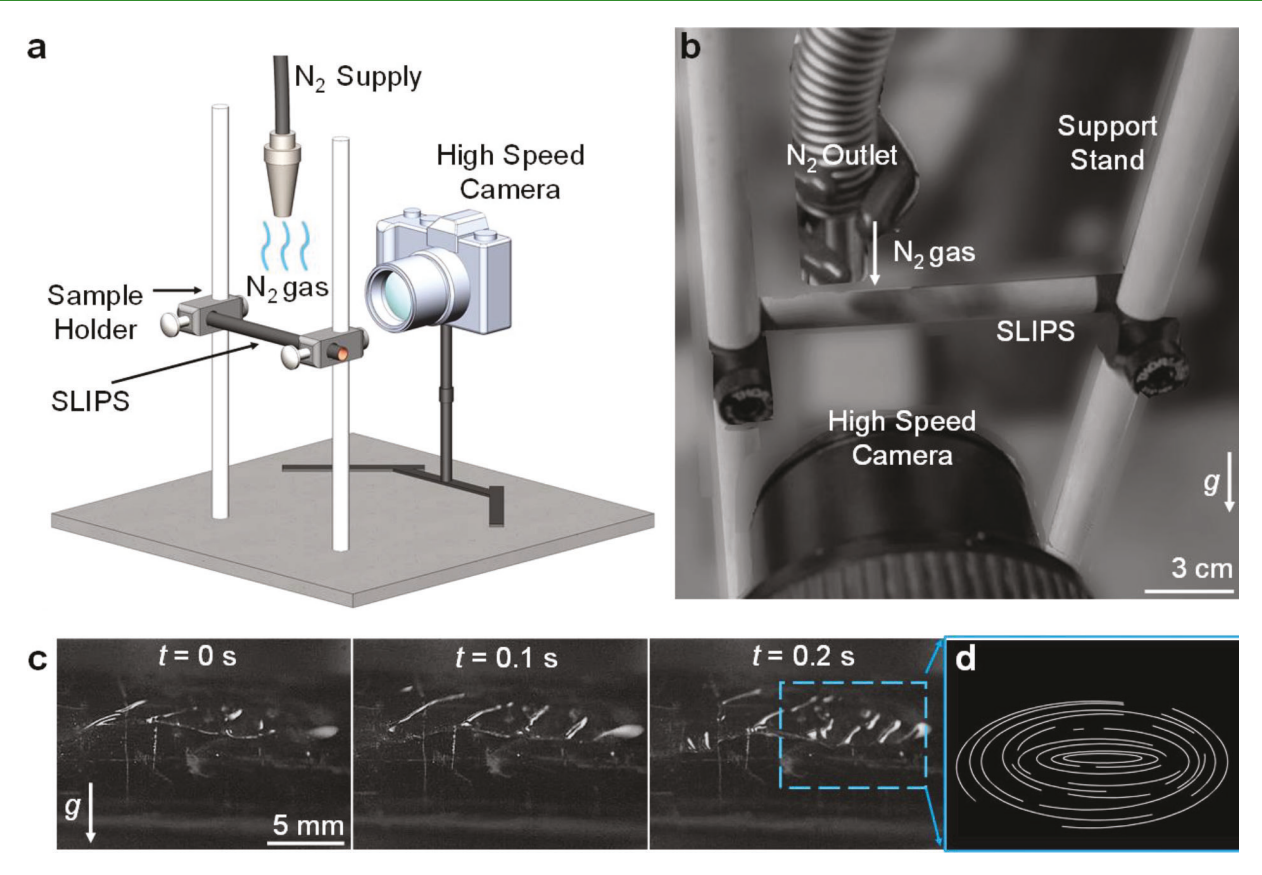


Figure 4. Gas shear durability testing. (a) Schematic (not to scale) and (b) image of the N_2 gas shear test apparatus for SLIPS tube samples. The N_2 gas is supplied on top of SLIPS from a gas cylinder through a nozzle having a 20 mm diameter, and visualization was performed with a high-speed camera from the side. (c) Time-lapse high-speed images of the SLIPS after exposure to N_2 gas impingement with a 10 m/s speed (pointing downward). The images show wrinkles forming in the thin oil layer due to the pressure distribution with no oil depletion (entrainment) observed. (d) Simplified schematic (not to scale) of oil wrinkles.

which acts to alter the condensate-sample surface energy during long-term exposure to condensation. As seen in Figure 2, after 20 days of steam condensation, F-Y25/6, K-1525, and K-16256 showed the formation of irregular-shaped droplets, demonstrating a slow transition to filmwise condensation within a week for the low viscosity SLIPS. Ethanol showed regular small condensate droplet formation at the very early stages of condensation (Figure 3, <1 day). For longer condensing times, the surfaces transitioned to a hybrid dropwise-filmwise condensation mode (Figure 3) which was stable in time. As seen in Figure 3, after 60 days of exposure to ethanol condensation, the high viscosity SLIPS showed the hybrid mode of condensation which is stable for K-1525 and F-Y25/6 for up to 5 months of exposure. The SLIPS impregnated with the highest viscosity oil (K-16256) held this hybrid stability for more than 8 months.

To quantify if the continual condensation durability tests affected the dropwise condensation heat transfer, the condensation heat transfer was measured after completing the 150 day ethanol condensation durability test. The condensation heat transfer coefficient measurement for pure ethanol was conducted in a separate controlled environmental chamber. The K-16256 SLIPS sample, which showed the best condensation durability, was measured to maintain the same condensation heat transfer coefficient as that of a freshly made sample, which was measured to be 7.3 \pm 3.1 kW/(m² K). The result is in line with the observations of continual dropwise condensation. Although we observed that oil

viscosity significantly alters SLIPSs durability, variation in oil viscosity does not affect the condensation heat transfer coefficient, as the coating thermal resistance for varying oils is significantly lower than the condensation heat transfer and internal single-phase convection heat transfer resistances (section S7 of the Supporting Information).

Durability to High-Speed Gas Shear. In a real shell-andtube condenser to be used in large-scale energy applications, vapor comes in contact via impingement with the condenser tubes at a certain velocity. 69 To ensure durability, SLIPS should withstand the potential vapor shear stemming from the incoming high velocity vapor to the condenser tubes. To evaluate the vapor shear resistance of SLIPS tubes, we performed high velocity air (N2 gas) shear tests on our fabricated tube samples. As shown in Figure 4a, SLIPS were first attached to a sample holder and placed horizontally to a stiff optical table. Clean N2 gas was supplied from a pressurized gas cylinder and guided on the top surface of the SLIPS (pointing down to the ground with gravity) through a nozzle. The oil layer deformation and possible oil depletion were monitored with a high-speed camera (Phantom v7.1, Vision Research) from the side (Figure 4a,b). Prior to testing, the flow velocity was measured and calibrated by using a hot wire an emometer. A flow velocity of $U_{gas} = 10 \text{ m/s}$ was used during testing based on the typical values of steam inlet velocity encountered in large-scale power generation surface condensers as well as petrochemical separation condensers.^{70,71} A SLIPS infused with K-1525 oil was selected due to its proven

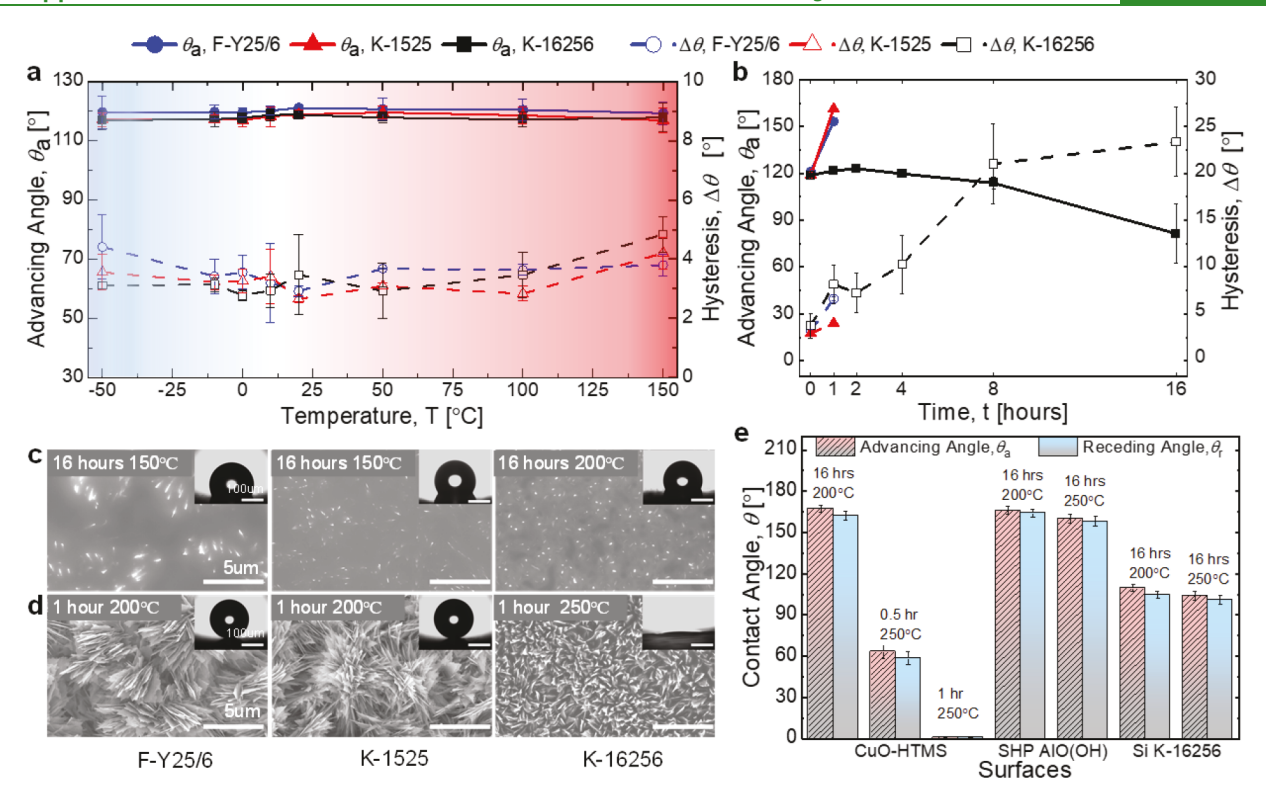


Figure 5. SLIPSs thermal stability in air. (a) Apparent advancing DI water contact angle (θ_a) and contact angle hysteresis ($\Delta\theta = \theta_a - \theta_r$) of F-Y256/6, K-1525, and K-16256 SLIPS for a wide range of air temperatures (-50 to 150 °C). (b) F-Y25/6 and K-1525 infused SLIPS become superhydrophobic (SHP) after exposing them to 200 °C air for 1 h. The K-16256 SLIPS begins to lose hydrophobicity at 200 °C, with complete failure at 250 °C. SEM images of (c) F-Y25/6 SLIPS after 16 h of exposure to 150 °C air, K-1525 SLIPS after 16 h of exposure to 150 °C air, and K-16256 SLIPS after 16 h of exposure to 200 °C air. The SEM images show the presence of oil infused within the CuO structured surfaces. SEM images of (d) F-Y25/6 SLIPS after 1 h of exposure to 200 °C air, K-1525 SLIPS after 1 h of exposure to 200 °C air, and K-16256 SLIPS after 1 h of exposure to 250 °C. (e) Contact angle change of Cu- and Si-based superhydrophobic and silicon-based SLIPSs. At 250 °C, the CuO surface starts to lose hydrophobicity and becomes completely superhydrophilic within 1 h of exposure.

durability in both steam and ethanol condensation. As shown in Figure 4c, even after exposing the surface to 10 m/s N_2 gas flow for a continual 90 min, no oil depletion was observed from the SLIPS. Only localized wrinkles formed (Figure 4c,d) due to gas shear forces at the N_2 gas exposed area due to the pressure distribution. These wrinkles disappeared after the gas shear force was removed due to self-healing of the lubricant driven by capillary pressure. Microgoniometric DI water contact angle measurement of a fresh sample and a 10 m/s N_2 gas exposed sample showed identical values of $\sim\!120^\circ$.

The lack of lubricant displacement from the tube can be understood through an analysis of the driving force for lubricant breakup, which can be quantified by the flow Weber number (We = $\rho_{gas}U_{gas}^2l/\gamma_{K-1525}$, where ρ_{gas} is the N₂ gas density, l is the structure pore radius (\sim 2 μ m), and γ_{K-1525} is the lubricant liquid-vapor surface tension (≈ 0.019 N/m). Here, We represents a ratio of the gas inertia force leading to lubricant breakup to the surface tension based capillary force keeping the lubricant within the structured surface pores. For the gas velocities tested here and the SLIPS surfaces chosen (K-1525), We < 0.009, well below We_{crit} = 0.75 required to break up the liquid film and entrain lubricant droplets in the gas flow.⁷² In fact, scaling reveals that the required gas velocities needed to initiate failure are $U_{crit} > 95$ m/s, which approaches the velocity at the exhaust of the steam turbine and which is limited by the National Electrical Manufacturers Association to 137 m/s.⁷⁰

Thermal Stability in Air. In addition to condensation durability, condensers undergoing manufacture or operation may encounter conditions where low or elevated ambient temperatures are encountered. For example, condenser tubing located near the shell-and-tube inlet can encounter superheated steam at high face velocities, significantly heating the surface and leading to degradation. To evaluate the durability of SLIPSs at both low and elevated temperatures, we selected and focused on the oils that were demonstrated to be durable to steam and ethanol condensation: F-Y25/6, K-1525, and K-16256. For the elevated temperature exposure experiments (50 to 250 °C), the samples were placed in an atmospheric pressure oven (Lindberg/Blue M Moldatherm Box Furnace). For low temperature exposure experiments $(-50 \text{ to } 10 \text{ }^{\circ}\text{C})$ the samples were placed in a freezer (Ult390-3-a31, Revco). At each temperature, five identical samples of each SLIPS were placed in the furnace or freezer. After 1 h of thermal exposure, the first sample was taken out, followed by the rest of the samples taken out sequentially at 2, 4, 8, and 16 h. After exposing the samples for a prescribed time and allowing the samples to equilibrate with the room temperature, the apparent advancing (θ_a) and receding (θ_r) DI water droplet contact angles were measured using the microgoniometer (MCA-3, Kyowa Interface Science).

As demonstrated in Figure 5a, the surfaces did not show any significant change in contact angle after exposing for 16 h at -50 to 150 °C. However, samples exposed to higher temperatures (>150 °C) showed changes in hydrophobicity.

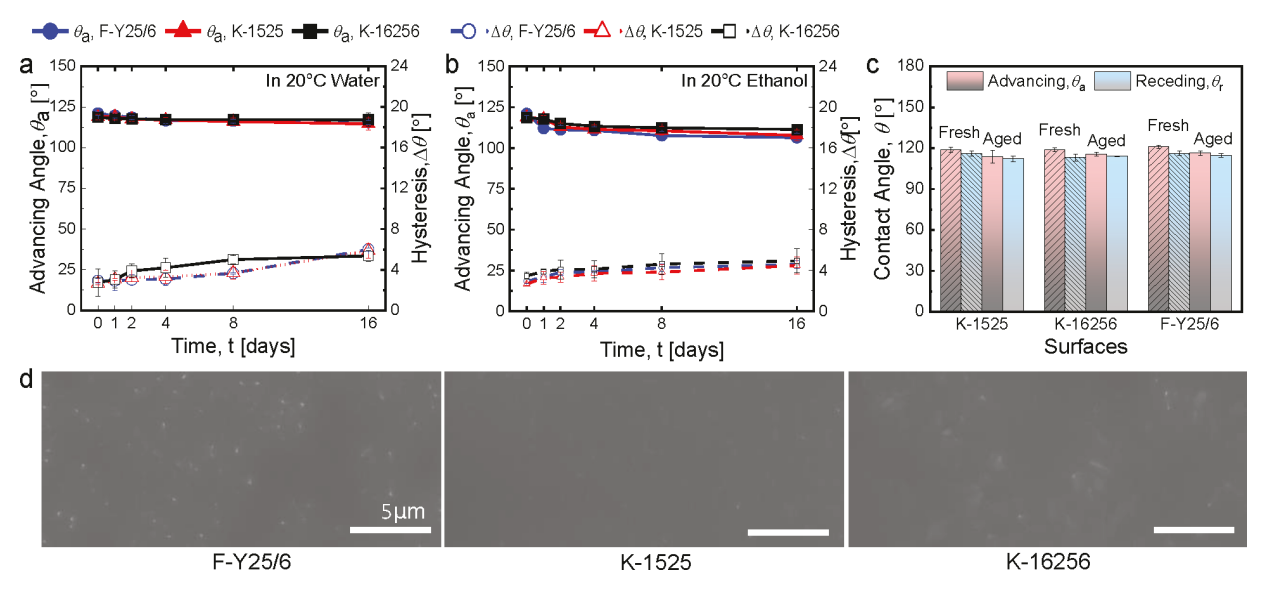


Figure 6. SLIPSs durability to prolonged condensate immersion. Advancing contact angle (θ_a) and contact angle hysteresis ($\Delta\theta$) of the SLIPSs surfaces after submerging in (a) 20 °C water and (b) 20 °C ethanol for a variety of different times. Legend is the same for (a) and (b) and is shown on top of (a, b). (c) Contact angle comparison of SLIPS infused with fresh oil and aged oil. Oil was aged by mixing it with ethanol and allowing it to rest for 12 months. Comparison shows no significant change in contact angle, depicting no property change of the oil as a response to prolonged ethanol exposure. (d) SEM images of SLIPSs samples after submerging them in ethanol for 16 days showing no apparent degradation of surface quality. Scale bars all represent 5 μ m.

The observed wettability change at high temperatures was independent of oil viscosity tested and did not result due to oil degradation. To verify this, we measured the room temperature oil viscosity after exposing the oils to elevated temperatures using a commercial rheometer (Table S2). Figure 5b shows that the F-Y25/6 and K-1525 infused SLIPSs become superhydrophobic after exposing the samples to 200 °C conditions for 1 h. The infused oil film evaporates at the elevated temperature,⁷⁴ leaving the silane-coated CuO exposed (Figure 5e). However, the K-16256 exposed to 200 °C did not lose all of its infused oil, showing only reduced hydrophobicity for longer exposure times (Figure 5b). This is due to the lower evaporation rate (vapor pressure) of more viscous Krytox 16256 oil, which fails to expose the CuO-HTMS base surface. After exposure of the samples to higher temperatures (250 °C) for 1 h, all samples became superhydrophilic (Figure 5b and Figure 5e, inset). The transition to superhydrophilicity occurs due to the majority of the oil evaporating (Figure 5e) in addition to the reference substrate CuO-HTMS desorbing its hydrophobic HTMS promoter.

To test our hypothesis, we fabricated a CuO-HTMS superhydrophobic surface and placed it in the same atmospheric pressure oven at 250 °C. As shown in Figure 5c, the superhydrophobic surface (CuO SHP) starts to degrade (reduced hydrophobicity) after 30 min of exposure to 250 °C air, failing completely within 1 h. To understand if the elevated temperature degradation is substrate dependent, we did the same experiments on a silicon wafer based superhydrophobic surface. A thin layer (~50 nm) of aluminum (Al) was sputtered (AJA3 Sputter) on a polished silicon wafer, which was then boehmized by immersing it in hot DI water at \sim 90 °C for 1 h (Figure S1), followed by HTMS salinization. ⁵⁶ Unlike CuO-HTMS, the Si-based superhydrophobic surface maintained excellent superhydrophobicity after 250 °C exposure due to stronger bonding of the silane to the native AlO(OH). Similar behavior was also observed on the SHP

samples made from Al tubing following the same boehmite formation (Figure S1) and salinization process. The results indicate that boehmite—HTMS has better thermal stability when compared to CuO—HTMS. Because of the better thermal stability of the Si-substrate boehmite surface, we also fabricated Si-based boehmite SLIPS by infusing Krytox 16256 (Si K-16256) following the same Si-based superhydrophobic boehmite fabrication process described previously. As shown in Figure 5c, after exposure of the Si-based boehmite SLIPS to 250 °C for 16 h, the surface maintained hydrophobicity.

The reason for the better SLIPS thermal stability of Si-based boehmite SLIPSs when compared to the CuO-based SLIPSs is due to two possible reasons. The first is due to the inherently different structure length scales of boehmite (<150 nm) and CuO-based (2 μ m) SLIPSs. The configuration of the lubricant infused in the microstructures is different, with the boehmite confining the lubricant to a much thinner region near the substrate.31 From our experimental observation of oil evaporation differences between the CuO microstructure and boehmite nanostructure, we note that the structure solid fraction of boehmite samples is higher than CuO (~0.023)⁵⁷ due to nanoscale porosity of boehmite,⁷⁵ resulting in slower oil evaporation rates. Although we hypothesize that slower oil evaporation occurs due to increased interaction between the structure and oil (closer proximity and higher interfacial area and capillary pressure), further work is needed to confirm this mechanism. The second reason for greater thermal stability is the higher surface coverage of the HTMS silane with boehmite when compared to CuO, which acts to slow the degradation of the underlying HTMS layer. As in the first mechanism, the second needs further work to verify the proposed hypothesis. See section S1 of the Supporting Information for additional details regarding the fabrication process of the Si-based boehmite SLIPS and Al-based boehmite SLIPS.

Durability to Condensate Flooding. Large shell and tube condensers collect the condensate product at the bottom

of the shell section, sometimes termed the hotwell. During operation, parts of the tubes near the hotwell may be inundated or completely immersed in the collecting condensate, resulting in prolonged times of direct immersion within the condensate, 76 requiring rigorous degradation quantification to single-phase liquid immersion conditions. To test SLIPSs durability during prolonged condensate exposure, we submerged the SLIPSs in a variety of different working fluids for extended time periods to characterize any change in functionality (contact angle). We simplified our tests by keeping the fluid stagnant while the surfaces were completely immersed in the fluid in a sealed container to reduce the rate of evaporation of the working fluid. For the test liquids, we selected room temperature (~20 $^{\circ}\text{C})$ water and ethanol. Test samples included the CuO-based SLIPSs infused with K-1525, K-16256, and F-Y25/6. During the room temperature water and ethanol test, five identical samples of each SLIPS were immersed in each liquid and sealed in separate glass bottles. After 1 day, the first sample of each type from each liquid was taken out followed by 2, 4, 8, and 16 days. Before submerging the samples, we changed the working fluids after each run to avoid possible contamination. After removal of the samples, drying was done on a hot plate at ~60 °C for 15 min followed by resting the samples at room temperature. After each test, when all samples reached room temperature, the apparent advancing (θ_a) and receding (θ_r) DI water droplet contact angles were measured on the microgoniometer (MCA-3, Kyowa Interface Science). More quantifiable methods of sample changes such as mass difference before and after immersion were difficult to measure due to limitations of available analytical balance mass scale sensitivity for the differences in mass obtained in the experiment.

As shown in Figures 6a,b, no observable change in contact angle of the SLIPS surfaces was observed in the tested immersion conditions. The SEM images showed the presence of the infused lubricant on the different SLIPS surfaces even after immersing them into the working fluids for 16 days (Figure 6d). To study the degradation of the infusing oil, we performed an oil aging experiment where each type of oil (K-1525, K-16256, and F-25/6) was mixed (50 vol %) with ethanol and kept in a sealed glass bottle for ~12 months. After the test, SLIPS samples were fabricated following the same CuO-HTMS surface fabrication followed by immersion in the aged oil mixtures followed by the same postimmersion treatment (oil drainage and drying). Then, the DI water contact angle of these samples was measured. As shown in Figure 6c, comparison of the SLIPS made with fresh infused oil with the SLIPS infused with the 12 months aged oil did not show any discernible difference in apparent contact angle behavior.

DISCUSSION

The results reported here have important implications for the potential development of scalable and robust surfaces for long-term dropwise condensation applications, both for steam and for low surface tension fluids. Systems that use refrigerants ^{77,78} and hydrocarbon fluids ^{79–81} stand to significantly benefit from dropwise condensation. Achieving stable dropwise condensation of steam on hydrophobic surfaces has a profound impact on global energy production, water conservation, and hence the carbon footprint of industrialized and developing nations. Dropwise condensation on durable hydrophobic condenser surfaces in shell and tube condensers of a thermoelectric or

I

nuclear power plant has the potential to lead to \sim 2% increase in overall power plant energy efficiency. Although the clear advantages of dropwise condensation have been understood for over a century, designing robust hydrophobic surfaces that can survive long-term operation with unchanged heat transfer performance has not been successful, severely limiting practical application.

Our work demonstrates the rational design of SLIPS for long-term stable dropwise condensation of both steam and ethanol condensation, indicating the importance of lubricant selection and degradation conditions. Our low temperature exposure durability study showed no change in wettability after exposure. However, exposing the surfaces to lower temperatures for extended periods (months) may alter these findings, especially if the surfaces are exposed for a long time near the pour point of the lubricant or at a lower temperature which may change the physical properties of the lubricant. The pour point of a lubricant is the lowest point at which it becomes too viscous and loses its flow properties. Pour points of K-1525, K-16256, and F-Y25/6 are −48, −15, and −35 °C, respectively. SLIPSs infused with these oils may show altered surface wettability if they are exposed to their respective pour point or lower temperatures for prolonged periods.

The condensation results demonstrating multimonth durability present a promising approach to enable the longterm operation of SLIPS condensers. Typical large scale condenser systems require multiyear longevity with continual operation. Some require more than a decade of operation prior to shutdown. The lack of miscibility between the lubricants studied here and the condensates tested presents an interesting opportunity to use active relubrication of the surfaces after prescribed time frames.⁵⁷ Compared to brushed lubricant impregnation, 83 our proposed contactless relubrication is attractive due to its simplicity. For example, the installation of spray nozzles capable of injecting lubricant into the steam inlet section of the condenser for relubrication presents a promising route to multiyear durability. The lack of miscibility enables the relatively easy separation of any drained lubricant outside of the condenser, which can be reused and resprayed on the external condenser tubing. In fact, past approaches to achieve durable dropwise condensation and corrosion protection have developed methods to apply additives to external condenser tubes by using similar approaches, demonstrating the added benefit of corrosion protection in addition to heat transfer enhancement.84

To evaluate the reusability of the multimonth durability tested samples after failure, we recoated the tested samples following the same SLIPS fabrication processes (section S1, Supporting Information) to emulate the proposed respray technique. For recoating, we selected the durable samples F-Y25/6, K-1525, and K-16256 from the ethanol condensation experiments. We conducted the same ethanol condensation experiment with the recoated samples, which showed stable dropwise condensation as was observed with the fresh samples (Figure S2). The findings indicate that long-term condensation exposure does not degrade the silane layer or underlying CuO structure. In fact, the oil layer acts as a protective shield to the silane layer, and the performance degradation of SLIPS mainly occurs due to oil depletion, which can be remedied by recoating. Although the revival of SLIPS performance with recoating reveals a clear added benefit of SLIPS over solid hydrophobic coatings, further studies are needed to compare the surface chemistry change between the freshly fabricated

and recoated SLIPSs after prolonged exposure and spray cycles.

Past studies have quantified the effect of oil viscosity on shear-driven surface failure focusing on external single-phase fluid flow. 85,86 Here, we experimentally prove that high viscosity oils can delay SLIPSs failure in the presence of condensate droplet shedding-driven oil depletion. Although higher oil viscosity enhances the life span of SLIPSs, future studies are needed that focus on the effects of oil viscosity, type of working fluid, and multidroplet coalescence dynamics on cloaking oil layer formation, oil ridge formation, and droplet shear dynamics, which all govern the coupled mechanics of lubricant depletion. Moreover, our study focused on CuObased superhydrophobic surfaces infused with different oils. Our high temperature air stability tests indicated that boehmite structures, due to their inherently different structure length scale when compared to CuO, result in enhanced life span at elevated temperatures. We hypothesize that this phenomenon occurs simply due to the higher surface roughness, nanoscale pore geometry, and enhanced surface interaction potential (thinner films). Future studies that can decouple the oil viscosity effects and nanostructure effects 87 (such as hierarchical surfaces with variable length scale roughness⁸⁸) are needed to evaluate the combined effect of oil viscosity and optimized structure on the improved life span of SLIPS in different degradation conditions.

CONCLUSIONS

In summary, we rigorously demonstrate the life span of a variety of SLIPSs in both water and ethanol condenser applications. The majority of SLIPSs show short life spans (<1 month) during steam condensation due to cloaking of the condensate by the infused lubricant. Among the tested samples, surfaces infused with the highest viscosity lubricant (Krytox-16256) exhibited dropwise condensation for up to 45 days. During ethanol condensation, SLIPSs infused with high viscosity lubricants (K-1525, F-Y25/6, and K-16256) showed stable dropwise condensation for multiple months due to the absence of cloaking, reducing oil depletion. Similar to steam condensation, the Krytox-16256 infused SLIPS was the most durable during ethanol condensation, demonstrating stable dropwise condensation for more than 8 months. To quantify durability to elevated temperatures as encountered by superheated gases in condensers, the K-1525 and F-Y25/6 infused SLIPSs showed good durability after exposure to 150 °C air for 16 h. The K-16256 infused surface was shown to be durable to 200 °C, finally degrading at 250 °C within 1 h. To quantify durability to immersion in a liquid, we subjected the SLIPSs to water and ethanol immersion conditions. All SLIPSs showed stable hydrophobicity even after 16 days of continual immersion. Our work presents design guidelines for the rational selection of lubricants for fabricating durable SLIPSs having wide applicability with both steam and ethanol condensation. Our results outline future directions toward the development of next-generation durable SLIPSs.

METHODS

Condensation Durability Test Setup. To evaluate the condensation durability of SLIPS for prolonged periods of time, we built a customized vacuum chamber which was mounted on a stainless-steel frame integrated on a movable cart (Figure 7a). The main environmental cylindrical chamber (16.5 in. diameter and 26 in. long) consists of a top opening, three customized side optical view

ports, and six apertures for various components around the side walls. The top opening was sealed with a rubber gasket and a custom-made stainless-steel view port (Kurt J. Lesker) which has three circular glass windows (two with a 6 in. diameter and the third with a 4.5 in. diameter). The top windows were used for visualization of the condensation phenomena inside the chamber. Among the six apertures, two were used as feedthrough connections to the chiller inlet and outlet, one was connected to the vacuum pump line, one was connected to a tee-joint for sensors and venting, and the other remaining two were sealed. All feedthroughs used high-vacuum compatible CF flanges having silver-plated copper gaskets. Other KF flanges were sealed with stainless steel centering rings accompanied by nitrile rubber O-rings.

A Cu tube in the form of a water jacket was soldered around the entire body of the chamber helically in the axial direction (Figure 7a,g), through which tap water at 65 °C was supplied from a hot water bath (1C1551256, PolyScience, Figure 7b). The hot water jacket helped to maintain the chamber wall temperature at ≈55 °C throughout the long-term experiment, which helped to reduce the amount of condensation occurring on the inside of the chamber wall and side view ports. A heater (3631K44, McMaster-Carr) with an adjustable temperature controller was wrapped around the outer wall of the chamber near the base occupied by the working fluid inside of the vessel (Figure 7g). A second tape heater (AWH-171-020, HTS/ Amptek) controlled with a variable voltage controller was attached to the outer-bottom surface of the chamber. These two heaters were calibrated and adjusted at voltages to maintain constant boiling of the working fluid inside of the chamber. The heating water jacket and all the heaters were insulated to limit heat losses to the ambient environment.

Cooling tap water was supplied to the chamber from a high-capacity chiller (N0772046, PolyScience) via the KF fluid feedthroughs (Kurt J. Lesker, Figure 7a,b). To monitor the water flow rate, an electromagnetic flow meter (FMG93-PVDF, Omega) with an accuracy of $\pm 1\%$ of the reading was integrated in series with the coolant inflow line (Figure 7e). To remove noncondensable gases prior to the experiments, a bellows valve (Ideal Vacuum) was attached to top of the environmental chamber for connection to a rotary vane vacuum pump (KJLC-RV212, Kurt J. Lesker, Figure 2c). An in-line liquid nitrogen (LN2) cooled trap (Kurt J. Lesker) was incorporated into the evacuation line from the environmental chamber to the vacuum pump via bellows tube connection (Kurt J. Lesker). The LN2 trap enabled removal of moisture from the air which also helped to produce a lower base pressure and faster pump down time (Figure 7b).

To monitor the pressure within the chamber, a vacuum pressure transducer (925 Micro Pirani, MKS) was installed (Figure 7d). A secondary valve (Kurt J. Lesker) was integrated with a tee flange between the pressure transducer and capped end to release the vacuum to ambient once the experiment was finished (Figure 7a,b). As the working fluid was poured into the chamber prior to pump down, complete removal of noncondensable gases (NCGs) was not possible. To monitor temperatures within the system, K-type thermocouple bundles were connected to the chamber via the thermocouple feedthroughs (Kurt J. Lesker). Outside of the chamber, two thermocouples monitored the inlet and outlet temperatures of the coolant. Inside of the chamber, the temperature of the side walls, vapor and ambient, and working fluid/condensate were monitored throughout the experiment.

The thermocouples, flow meter, and pressure transducer were electrically connected to a data acquisition (DAQ) system (cDAQ-9174, National Instruments), and data were continuously recorded throughout the experiment with all collected data analyzed with LabVIEW. The DAQ system included a thermocouple input module (NI-9213, National Instruments), a digital module (NI-9423, National Instruments), a voltage input module (NI-9209, National Instruments), and a terminal block (NI-9923, National Instruments). A stainless steel manifold (Swagelok) was built to hold the test samples. Care was taken while making the manifold so that none of the samples resided in the same vertical plane (Figure 7h).

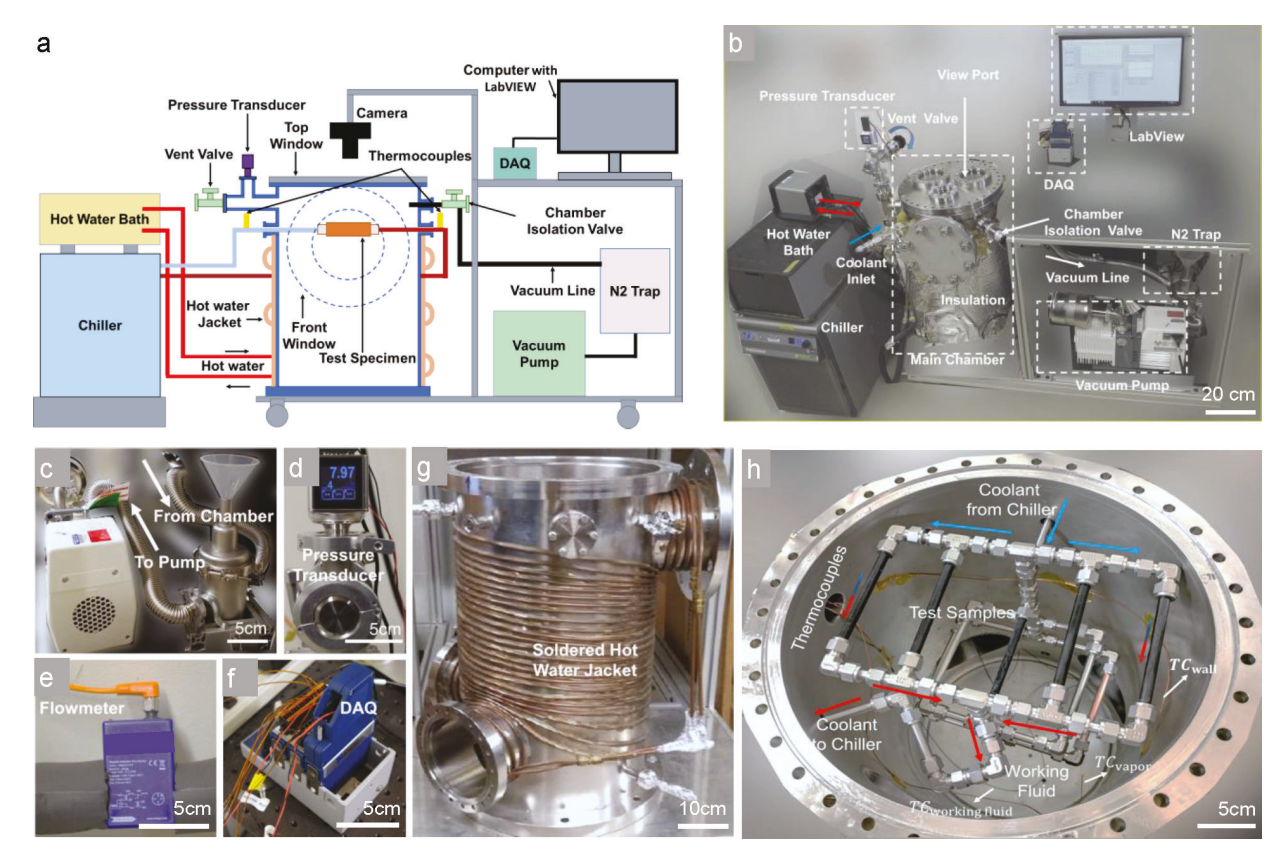


Figure 7. Condensation chamber for durability experiments. (a) Schematic (not to scale) and (b) image of the test rig showing all system components. (c) Vacuum line showing the flow path from the main chamber to the vacuum pump, where the LN2 trap is placed. Photograph of the (d) pressure transducer, (e) flowmeter, and (f) DAQ system. (g) Photograph showing the Cu tube water jacket soldered on the main chamber, helping to reduce condensate accumulation on the chamber walls. (h) Photograph of the Swagelok manifold built for holding the test tube samples.

Furthermore, manifold design was such that close hydraulic balancing (equivalent flow lengths) was achieved for each sample to ensure similar coolant flow rates for all tube samples. This prevented condensate drainage from top samples to lower samples. Finally, a DSLR camera (K-50, Pentax) was placed outside of the top view port of the chamber for visual observation of coating degradation (Figure 7a).

A set of strict test procedures were followed to ensure consistency throughout the experiments. First, the chamber interior was thoroughly cleaned with isopropyl alcohol (IPA) to remove any contaminants. Then the chamber was filled with 15 L of the working fluid (DI water or ethanol). The hot water bath (Cu jacket heater) and tape heaters were turned on to heat up the chamber walls for drying out inside of the chamber prior to pump down and to prevent condensation during the experiments. The test samples were fixed by using Swagelok connections to the customized manifolds holding the samples. The manifolds were then connected to the coolant loop via the inlet and outlet feedthroughs (Figure 7h). Simultaneously, thermocouples were attached to the chamber walls by using Cu tape and placed inside the working fluid residing on bottom.

Condensation Durability Testing Protocols. Given the long period of continuous condensation (>1 month), a leak test was performed to ensure no leaks were present before each experimental trial. After sealing all openings, we closed all valves of the chamber. The LN2 trap was first filled with liquid nitrogen. After closing the vent valve, we turned the pump on, and then the valve connecting the bellows to the vacuum pump via the LN2 trap was slowly opened to initiate the pump-down process. The chamber pressure was monitored by a pressure transducer (Figure S2a,b). In the middle of the pump-down process, the chiller was turned on, and the water temperature was set to 5 °C. The inflow rate of the coolant was monitored by using the electromagnetic flowmeter and was

maintained at 10 LPM. The pump-down process took $\sim\!30$ min to achieve a vacuum level of $P\sim5$ kPa. Because of the presence of the working fluid in the chamber, it is not possible to completely remove all NCGs unless a full freeze–pump—thaw cycle was enacted. However, the partial vacuum conditions reached were maintained in the chamber which reduced the amount of heat required to boil the working fluids. Whenever necessary during pump down, the LN2 trap was refilled. The LN2 trap was cleaned midway, since frost formed on the LN2 trap and blocked the vacuum line during the pump-down process.

When a steady base pressure was achieved, the valve connecting the environmental chamber and the LN2 trap was closed, and the pump was turned off. Then, the valve connecting the vacuum pump and the ambient was opened to release the vacuum in the pump line. Before conducting the experiment, the leak test was performed. At that time, the chamber was filled with the required amount of working fluid, and dummy samples were connected to the Swagelok manifolds. For the leak test, the chamber was left in the vacuum state for >24 h, and the chamber pressure was monitored with the pressure transducer. The leak rate was characterized to acquire the leak rate of air into the chamber. When the leak test was finished, the vacuum was released by opening the valve connecting the environmental chamber and the ambient. Once the leak test was finished, an actual experiment was performed. In actual experiments, steady-state conditions were typically reached after approximately 30-40 min of operation. Steady-state operating parameters are shown in Figure S2a,b. Throughout the experiments, data (temperatures, pressure, and flow rate) were collected, and the images of each sample were recorded by using the DSLR camera. To maintain the same level of pressure though the long-tern durability test, the condensation rig had to be shut down once per month to pump down the chamber to the desired pressure level to remove noncondensable gases. This was done due to

air leaking into the chamber at a slow rate from the atmosphere-to-saturated vapor (subatmospheric pressure) pressure difference. Furthermore during shutdown, the chamber was not opened, and only the cooling water flowing through the tubes was arrested. During shutdown, the chamber was vacuumed through a valve feedthrough to remove noncondensable gases, with shutdown lasting no more than 3 h per month. For the remaining time, continual 24 h a day condensation occurred in the chamber.

ASSOCIATED CONTENT

Supporting Information

The Supporting Information is available free of charge at https://pubs.acs.org/doi/10.1021/acsami.1c17010.

Details of sample fabrication (section S1); properties of infused oil (section S2); effect of exposure temperature on oil viscosity (section S3); scaling analysis of potential oil depletion mechanisms (section S4); SEM images (section S5); relubricated SLIPS samples (section S6); effect of oil viscosity to the heat transfer coefficient (section S7); durability chamber operation (section S8) (PDF)

AUTHOR INFORMATION

Corresponding Author

Nenad Miljkovic — Department of Mechanical Science and Engineering, University of Illinois, Urbana, Illinois 61801, United States; Materials Research Laboratory and Department of Electrical and Computer Engineering, University of Illinois, Urbana, Illinois 61801, United States; International Institute for Carbon Neutral Energy Research (WPI-I2CNER), Kyushu University, Fukuoka 819-0395, Japan; orcid.org/0000-0002-0866-3680; Email: nmiljkov@illinois.edu

Authors

Muhammad Jahidul Hoque — Department of Mechanical Science and Engineering, University of Illinois, Urbana, Illinois 61801, United States; orcid.org/0000-0002-8036-4511

Soumyadip Sett – Department of Mechanical Science and Engineering, University of Illinois, Urbana, Illinois 61801, United States

Xiao Yan – Department of Mechanical Science and Engineering, University of Illinois, Urbana, Illinois 61801, United States; Oorcid.org/0000-0001-9948-3468

Derrick Liu — Department of Mechanical Science and Engineering, University of Illinois, Urbana, Illinois 61801, United States

Kazi Fazle Rabbi — Department of Mechanical Science and Engineering, University of Illinois, Urbana, Illinois 61801, United States; orcid.org/0000-0003-3630-1625

Haoyun Qiu — Department of Mechanical Science and Engineering, University of Illinois, Urbana, Illinois 61801, United States

Mansoor Qureshi – Department of Chemistry, University of Illinois, Urbana, Illinois 61801, United States

George Barac – BP International Limited, Naperville, Illinois 60563, United States

Leslie Bolton – BP plc, Sunbury-on-Thames, Middlesex TW16 7LN, U.K.

Complete contact information is available at: https://pubs.acs.org/10.1021/acsami.1c17010

Author Contributions

N.M. conceived the idea for the work and guided the work. Building of the durability chamber setup was done by M.J.H. with the supervision of N.M. Sample fabrication was performed by M.J.H., S.S., X.Y., and K.R. Sample characterization was performed by M.J.H., D.L., M.Q., and H.Q. Durability experiments were performed by M.J.H., S.S., and X.Y. Data analysis was performed by M.J.H., D.L., X.Y., and S.S. with help of G.B., L.B., and N.M. All authors discussed the results. M.J.H. and N.M. wrote the manuscript. All authors approved the submission of the manuscript.

Notes

The authors declare no competing financial interest.

ACKNOWLEDGMENTS

M.J.H. and N.M. gratefully acknowledge funding support from the Office of Naval Research (ONR) under Grant N00014-16-1-2625. N.M. also gratefully acknowledges funding support from the International Institute for Carbon Neutral Energy Research (WPI-I2CNER), sponsored by the Japanese Ministry of Education, Culture, Sports, Science and Technology. This research was partially supported by the NSF through the University of Illinois at Urbana—Champaign Materials Research Science and Engineering Center (DMR-1720633).

REFERENCES

- (1) Barthlott, W.; Neinhuis, C. Purity of the Sacred Lotus, or Escape from Contamination in Biological Surfaces. *Planta* **1997**, 202, 1–8.
- (2) Miljkovic, N.; Enright, R.; Nam, Y.; Lopez, K.; Dou, N.; Sack, J.; Wang, E. N. Jumping-Droplet-Enhanced Condensation on Scalable Superhydrophobic Nanostructured Surfaces. *Nano Lett.* **2013**, *13* (1), 179–187.
- (3) Tuteja, A.; Choi, W.; Ma, M.; Mabry, J. M.; Mazzella, S. A.; Rutledge, G. C.; McKinley, G. H.; Cohen, R. E. Designing Superoleophobic Surfaces. *Sceince* **2007**, *318*, 1618–1622.
- (4) Sun, T.; Feng, L.; Gao, X.; Jiang, L. Bioinspired Surfaces with Special Wettability. Acc. Chem. Res. 2005, 38 (8), 644-652.
- (5) Feng, L.; Li, S.; Li, Y.; Li, H.; Zhang, L.; Zhai, J.; Song, Y.; Liu, B.; Jiang, L.; Zhu, D. Super-Hydrophobic Surfaces: From Natural to Artificial. *Adv. Mater.* **2002**, *14* (24), 1857–1860.
- (6) Quéré, D. Non-Sticking Drops. Rep. Prog. Phys. 2005, 68 (11), 2495–2532.
- (7) Lafuma, A.; Quere, D. Superhydrophobic States. *Nat. Mater.* **2003**, 2 (7), 457–460.
- (8) Narhe, R. D.; Beysens, D. A. Nucleation and Growth on a Superhydrophobic Grooved Surface. *Phys. Rev. Lett.* **2004**, 93 (7), 076103.
- (9) Wier, K. A.; McCarthy, T. J. Condensation on Ultrahydrophobic Surfaces and Its Effect on Droplet Mobility: Ultrahydrophobic Surfaces Are Not Always Water Repellant. *Langmuir* **2006**, *22*, 2433–2436.
- (10) Enright, R.; Miljkovic, N.; Al-Obeidi, A.; Thompson, C. V.; Wang, E. N. Condensation on Superhydrophobic Surfaces: The Role of Local Energy Barriers and Structure Length Scale. *Langmuir* **2012**, 28 (40), 14424–14432.
- (11) Cha, H.; Wu, A.; Kim, M. K.; Saigusa, K.; Liu, A.; Miljkovic, N. Nanoscale-Agglomerate-Mediated Heterogeneous Nucleation. *Nano Lett.* **2017**, *17* (12), 7544–7551.
- (12) Ma, J.; Cha, H.; Kim, M. K.; Cahill, D. G.; Miljkovic, N. Condensation Induced Delamination of Nanoscale Hydrophobic Films. *Adv. Funct. Mater.* **2019**, 29 (43), 1905222.
- (13) Bocquet, L.; Lauga, E. A Smooth Future? *Nat. Mater.* **2011**, *10* (5), 334–337.
- (14) Varanasi, K. K.; Deng, T.; Smith, J. D.; Hsu, M.; Bhate, N. Frost Formation and Ice Adhesion on Superhydrophobic Surfaces. *Appl. Phys. Lett.* **2010**, *97* (23), 234102.

- (15) Wen, L.; Tian, Y.; Jiang, L. Bioinspired Super-Wettability from Fundamental Research t Practical Applications. *Angew. Chem., Int. Ed. Engl.* **2015**, 54 (11), 3387–3399.
- (16) Wu, Y.; Feng, J.; Gao, H.; Feng, X.; Jiang, L. Superwettability-Based Interfacial Chemical Reactions. *Adv. Mater.* **2019**, *31* (8), 1800718.
- (17) Sigal, G. B.; Mrksich, M.; Whitesides, G. M. Effect of Surface Wettability on the Adsorption of Proteins and Detergents. *J. Am. Chem. Soc.* **1998**, *120*, 3464–3473.
- (18) Darouiche, R. O. Device-Associated Infections: A Macroproblem that Starts with Microadherence. *Clinal Infectious Diseases* **2001**, *33*, 1567–1572.
- (19) Nhung Nguyen, T. P.; Brunet, P.; Coffinier, Y.; Boukherroub, R. Quantitative Testing of Robustness on Superomniphobic Surfaces by Drop Impact. *Langmuir* **2010**, *26* (23), 18369–18373.
- (20) Liu, T.; Kim, C.-J. Turning a Surface Superrepellent Even to Completely Wetting Liquids. *Science* **2014**, *346* (6213), 1096–1100.
- (21) Weisensee, P. B.; Torrealba, E. J.; Raleigh, M.; Jacobi, A. M.; King, W. P. Hydrophobic and Oleophobic Re-Entrant Steel Microstructures Fabricated Using Micro Electrical Discharge Machining. J. Micromech. Microeng. 2014, 24 (9), 095020.
- (22) Wilke, K. L.; Preston, D. J.; Lu, Z.; Wang, E. N. Toward Condensation-Resistant Omniphobic Surfaces. ACS Nano 2018, 12 (11), 11013–11021.
- (23) Golden, J. S.; Handfield, R.; Pascual-Gonzalez, J.; Agsten, B.; Brennan, T.; Khan, L.; True, E. *Indicators of the U.S. Biobased Economy*; United States Department of Agriculture: 2018; pp 1–74.
- (24) Lammens, T. M.; Franssen, M. C. R.; Scott, E. L.; Sanders, J. P. M. Availability of Protein-Derived Amino Acids as Feedstock for the Production of Bio-Based Chemicals. *Biomass and Bioenergy* **2012**, *44*, 168–181.
- (25) Miao, X.; Wu, Q. Biodiesel Production from Heterotrophic Microalgal Oil. *Bioresour. Technol.* **2006**, 97 (6), 841–846.
- (26) Ma, J.; Sett, S.; Cha, H.; Yan, X.; Miljkovic, N. Recent Developments, Challenges, and Pathways to Stable Dropwise Condensation: A Perspective. *Appl. Phys. Lett.* **2020**, *116* (26), 260501.
- (27) Agonafer, D.; Spector, M. S.; Miljkovic, N. Materials and Interface Challenges in High-Vapor-Quality Two-Phase Flow Boiling Research. *IEEE Transactions on Components, Packaging and Manufacturing Technology* **2021**, *11* (10), 1583–1591.
- (28) Suh, Y.; Lee, J.; Simadiris, P.; Yan, X.; Sett, S.; Li, L.; Rabbi, K. F.; Miljkovic, N.; Won, Y. A Deep Learning Perspective on Dropwise Condensation. *Adv. Sci.* **2021**, *8*, e2101794.
- (29) Wong, T. S.; Kang, S. H.; Tang, S. K.; Smythe, E. J.; Hatton, B. D.; Grinthal, A.; Aizenberg, J. Bioinspired Self-Repairing Slippery Surfaces with Pressure-Stable Omniphobicity. *Nature* **2011**, 477 (7365), 443–447.
- (30) Lafuma, A.; Quéré, D. Slippery Pre-Suffused Surfaces. EPL (Europhysics Letters) 2011, 96 (5), 56001.
- (31) Smith, J. D.; Dhiman, R.; Anand, S.; Reza-Garduno, E.; Cohen, R. E.; McKinley, G. H.; Varanasi, K. K. Droplet Mobility on Lubricant-Impregnated Surfaces. *Soft Matter* **2013**, *9* (6), 1772–1780.
- (32) Weisensee, P. B.; Wang, Y.; Qian, H.; Schultz, D.; King, W. P.; Miljkovic, N. Condensate Droplet Size Distribution on Lubricant-Infused Surfaces. *Int. J. Heat Mass Transfer* **2017**, *109*, 187–199.
- (33) Ge, Q.; Raza, A.; Li, H.; Sett, S.; Miljkovic, N.; Zhang, T. Condensation of Satellite Droplets on Lubricant-Cloaked Droplets. ACS Appl. Mater. Interfaces 2020, 12 (19), 22246–22255.
- (34) Preston, D. J.; Lu, Z.; Song, Y.; Zhao, Y.; Wilke, K. L.; Antao, D. S.; Louis, M.; Wang, E. N. Heat Transfer Enhancement During Water and Hydrocarbon Condensation on Lubricant Infused Surfaces. Sci. Rep 2018, 8 (1), 540.
- (35) Rykaczewski, K.; Paxson, A. T.; Staymates, M.; Walker, M. L.; Sun, X.; Anand, S.; Srinivasan, S.; McKinley, G. H.; Chinn, J.; Scott, J. H.; Varanasi, K. K. Dropwise Condensation of Low Surface Tension Fluids on Omniphobic Surfaces. *Sci. Rep.* **2015**, *4*, 4158.

- (36) Anand, S.; Paxson, A. T.; Dhiman, R.; Smith, J. D.; Varanasi, K. K. Enhanced Condensation on Lubricant-Impregnated Nanotextured Surfaces. *ACS Nano* **2012**, *6* (11), 10122–10129.
- (37) Liu, Z.; Preston, D. J. Enhanced Condensation for Improved Energy Efficiency. *Joule* **2019**, 3 (5), 1182–1184.
- (38) Park, K. C.; Kim, P.; Grinthal, A.; He, N.; Fox, D.; Weaver, J. C.; Aizenberg, J. Condensation on Slippery Asymmetric Bumps. *Nature* **2016**, *531* (7592), 78–82.
- (39) Sett, S.; Sokalski, P.; Boyina, K.; Li, L.; Rabbi, K. F.; Auby, H.; Foulkes, T.; Mahvi, A.; Barac, G.; Bolton, L. W.; Miljkovic, N. Stable Dropwise Condensation of Ethanol and Hexane on Rationally Designed Ultrascalable Nanostructured Lubricant-Infused Surfaces. *Nano Lett.* **2019**, *19* (8), 5287–5296.
- (40) Erb, R.; Thelen, E. Promoting Permanent Dropwise Condensation. *Ind. Eng. Chem.* **1965**, *57* (10), 49–52.
- (41) Marto, P. J.; Looney, D. J.; Rose, J. W.; Wanniarachchi, A. S. Evaluation of organic coatings for the promotion of dropwise condensation of steam. *Int. J. Heat Mass Transfer* **1986**, 29 (8), 1109–1117.
- (42) Holden, K. M.; Wanniarachchi, A. S.; Marto, P. J.; Boone, D. H.; Rose, J. W. The Use of Organic Coatings to Promote Dropwise Condensation of Steam. *J. Heat Transfer* **1987**, *109* (3), 768–774.
- (43) Erb, R. A. Dropwise condensation on gold. *Gold Bulletin* **1973**, 6 (1), 2–6.
- (44) Haraguchi, T.; Shimada, R.; Kumagai, S.; Takeyama, T. The effect of polyvinylidene chloride coating thickness on promotion of dropwise steam condensation. *Int. J. Heat Mass Transfer* **1991**, 34 (12), 3047–3054.
- (45) Vemuri, S.; Kim, K. J.; Wood, B. D.; Govindaraju, S.; Bell, T. W. Long term testing for dropwise condensation using self-assembled monolayer coatings of n-octadecyl mercaptan. *Applied Thermal Engineering* **2006**, *26* (4), 421–429.
- (46) Ma, J.; Porath, L. E.; Haque, M. F.; Sett, S.; Rabbi, K. F.; Nam, S.; Miljkovic, N.; Evans, C. M. Ultra-Thin Self-Healing Vitrimer Coatings for Durable Hydrophobicity. *Nat. Commun.* **2021**, *12* (1), 5210.
- (47) Ouyang, Y.; Zhao, J.; Qiu, R.; Hu, S.; Zhang, Y.; Wang, P. Bioinspired Superhydrophobic and Oil-Infused Surface: Which is the Better Choice to Prevent Marine Biofouling? *Colloids Surf., A* **2018**, 559, 297–304.
- (48) Tenjimbayashi, M.; Park, J. Y.; Muto, J.; Kobayashi, Y.; Yoshikawa, R.; Monnai, Y.; Shiratori, S. In Situ Formation of Slippery-Liquid-Infused Nanofibrous Surface for a Transparent Antifouling Endoscope Lens. *ACS Biomater Sci. Eng.* **2018**, *4* (5), 1871–1879.
- (49) Bandyopadhyay, S.; Khare, S.; Bhandaru, N.; Mukherjee, R.; Chakraborty, S. High Temperature Durability of Oleoplaned Slippery Copper Surfaces. *Langmuir* **2020**, *36* (15), 4135–4143.
- (50) Yu, P.; Lian, Z.; Xu, J.; Yu, H. Slippery Liquid Infused Porous Surfaces with Corrosion Resistance Potential on Aluminum Alloy. *RSC Adv.* **2021**, *11* (2), 847–855.
- (51) Goodband, S. J.; Armstrong, S.; Kusumaatmaja, H.; Voi Tchovsky, K. Effect of Ageing on the Structure and Properties of Model Liquid-Infused Surfaces. *Langmuir* **2020**, *36* (13), 3461–3470.
- (52) Lee, J.; Shin, S.; Jiang, Y.; Jeong, C.; Stone, H. A.; Choi, C. H. Oil-Impregnated Nanoporous Oxide Layer for Corrosion Protection with Self-Healing. *Adv. Funct. Mater.* **2017**, *27* (15), 1606040.
- (53) Gurav, A. B.; Shi, H. X.; Duan, M.; Pang, X. L.; Li, X. G. Highly transparent, hot water and scratch resistant, lubricant-infused slippery surfaces developed from a mechanically-weak superhydrophobic coating. *Chemical Engineering Journal* **2021**, *416*, 127809.
- (54) Khodakarami, S.; Zhao, H.; Rabbi, K. F.; Miljkovic, N. Scalable Corrosion-Resistant Coatings for Thermal Applications. *ACS Appl. Mater. Interfaces* **2021**, *13* (3), 4519–4534.
- (55) Hoque, M. J.; Yan, X.; Keum, H.; Li, L.; Cha, H.; Park, J. K.; Kim, S.; Miljkovic, N. High-Throughput Stamping of Hybrid Functional Surfaces. *Langmuir* **2020**, *36* (21), 5730–5744.
- (56) Yang, Z.; Wu, Y.-Z.; Ye, Y.-F.; Gong, M.-G.; Xu, X.-L. A Simple Way to Fabricate an Aluminum Sheet with Superhydrophobic and Self-Cleaning Properties. *Chinese Physics B* **2012**, *21* (12), 126801.

- (57) Sett, S.; Oh, J.; Cha, H.; Veriotti, T.; Bruno, A.; Yan, X.; Barac, G.; Bolton, L. W.; Miljkovic, N. Lubricant-Infused Surfaces for Low-Surface-Tension Fluids: The Extent of Lubricant Miscibility. ACS Appl. Mater. Interfaces 2021, 13 (19), 23121–23133.
- (58) Sett, S.; Yan, X.; Barac, G.; Bolton, L. W.; Miljkovic, N. Lubricant-Infused Surfaces for Low-Surface-Tension Fluids: Promise versus Reality. *ACS Appl. Mater. Interfaces* **2017**, 9 (41), 36400–36408.
- (59) Yan, X.; Chen, F.; Sett, S.; Chavan, S.; Li, H.; Feng, L.; Li, L.; Zhao, F.; Zhao, C.; Huang, Z.; Miljkovic, N. Hierarchical Condensation. ACS Nano 2019, 13 (7), 8169–8184.
- (60) Yan, X.; Zhang, L.; Sett, S.; Feng, L.; Zhao, C.; Huang, Z.; Vahabi, H.; Kota, A. K.; Chen, F.; Miljkovic, N. Droplet Jumping: Effects of Droplet Size, Surface Structure, Pinning, and Liquid Properties. ACS Nano 2019, 13 (2), 1309–1323.
- (61) Yan, X.; Huang, Z.; Sett, S.; Oh, J.; Cha, H.; Li, L.; Feng, L.; Wu, Y.; Zhao, C.; Orejon, D.; Chen, F.; Miljkovic, N. Atmosphere-Mediated Superhydrophobicity of Rationally Designed Micro/Nanostructured Surfaces. ACS Nano 2019, 13 (4), 4160–4173.
- (62) Harkins, W. D.; Feldman, A. Films.. The Spreading of Liquids and the Spreading Coefficient. *J. Am. Chem. Soc.* **1922**, 44, 2665–2685.
- (63) Günay, A. A.; Sett, S.; Ge, Q.; Zhang, T.; Miljkovic, N. Cloaking Dynamics on Lubricant-Infused Surfaces. *Advanced Materials Interfaces* **2020**, 7 (19), 2000983.
- (64) Preston, D. J.; Song, Y.; Lu, Z.; Antao, D. S.; Wang, E. N. Design of Lubricant Infused Surfaces. ACS Appl. Mater. Interfaces 2017, 9 (48), 42383–42392.
- (65) Adera, S.; Alvarenga, J.; Shneidman, A. V.; Zhang, C. T.; Davitt, A.; Aizenberg, J. Depletion of Lubricant from Nanostructured Oil-Infused Surfaces by Pendant Condensate Droplets. *ACS Nano* **2020**, 14 (7), 8024–8035.
- (66) Kreder, M. J.; Daniel, D.; Tetreault, A.; Cao, Z. L.; Lemaire, B.; Timonen, J. V. I.; Aizenberg, J. Film Dynamics and Lubricant Depletion by Droplets Moving on Lubricated Surfaces. *Physical Review X* **2018**, *8* (3), 031053.
- (67) Miljkovic, N.; Enright, R.; Wang, E. N. Modeling and Optimization of Superhydrophobic Condensation. *Journal of Heat Transfer* **2013**, *135* (11), 111004.
- (68) Cha, H.; Vahabi, H.; Wu, A.; Chavan, S.; Kim, M. K.; Sett, S.; Bosch, S. A.; Wang, W.; Kota, A. K.; Miljkovic, N. Dropwise condensation on solid hydrophilic surfaces. *Sci. Adv.* **2020**, *6* (2), eaax0746.
- (69) Yau, K. K.; Cooper, J. R.; Rose, J. W. Effect of Fin Spacing on the Performance of Horizontal Integral-Fin Condenser Tubes. *Journal of Heat Transfer-Transactions of the Asme* **1985**, *107* (2), 377–383.
- (70) Spencer, E. Specifying Steam Surface Condensers; Graham Mfg.Co., Inc.: Great Neck, Long Island, NY.
- (71) Silver, R. S. An Approach to a General Theory of Surface Condensers. *Proc. Instn Mech Engrs* **1963**, 178 (1), 339–357.
- (72) Faghri, A. Heat Pipe Science and Technology; Global Digital Press: 2016.
- (73) Saunders, E. A. D. Heat Exchanges: Selection, Design and Construction; Longman Scientific and Technical: New York, 1988.
- (74) Zhang, J.; Wu, L.; Li, B.; Li, L.; Seeger, S.; Wang, A. Evaporation-induced transition from Nepenthes pitcher-inspired slippery surfaces to lotus leaf-inspired superoleophobic surfaces. *Langmuir* **2014**, *30* (47), 14292–9.
- (75) Li, L.; Lin, Y.; Rabbi, K. F.; Ma, J.; Chen, Z.; Patel, A.; Su, W.; Ma, X.; Boyina, K.; Sett, S.; Mondal, D.; Tomohiro, N.; Hirokazu, F.; Miljkovic, N. Fabrication Optimization of Ultra-Scalable Nanostructured Aluminum-Alloy Surfaces. ACS Appl. Mater. Interfaces 2021, 13 (36), 43489–43504.
- (76) Armstrong Fluid Handling, I. Understanding and Solving Equipment Stall, 2021.
- (77) Park, K.-J.; Seo, T.; Jung, D. Performance of alternative refrigerants for residential air-conditioning applications. *Applied energy* **2007**, *84* (10), 985–991.

- (78) Cavallini, A.; Censi, G.; Del Col, D.; Doretti, L.; Longo, G.; Rossetto, L.; Zilio, C. Condensation inside and outside smooth and enhanced tubes—a review of recent research. *International Journal of Refrigeration* **2003**, 26 (4), 373–392.
- (79) Allen, D. T.; Shonnard, D. R. Green Engineering: Environmentally Conscious Design of Chemical Processes; Pearson Education: 2001.
- (80) Koppejan, J.; Van Loo, S. The Handbook of Biomass Combustion and Co-firing; Routledge: 2012.
- (81) Sun, D.-W.; Zheng, L. Vacuum cooling technology for the agrifood industry: Past, present and future. *Journal of food engineering* **2006**, 77 (2), 203–214.
- (82) Khalil, K.; Soto, D.; Farnham, T.; Paxson, A.; Katmis, A. U.; Gleason, K.; Varanasi, K. K. Grafted Nanofilms Promote Dropwise Condensation of Low-Surface-Tension Fluids for High-Performance Heat Exchangers. *Joule* **2019**, *3* (5), 1377–1388.
- (83) Seo, D.; Shim, J.; Lee, C.; Nam, Y. Brushed lubricant-impregnated surfaces (BLIS) for long-lasting high condensation heat transfer. *Sci. Rep* **2020**, *10* (1), 2959.
- (84) Hoenig, S. H.; B, M.; Robinson, G.; Pierce, C.; Meskers, D.; Ellis, M. C.; Bonner, R. W., III. Technoeconomic Benefits of Film-Forming Amine Products Applied to Stea, Surface Condensers. *PPCHEM J.* **2021**, 23 (1), 4–16.
- (85) Wexler, J. S.; Jacobi, I.; Stone, H. A. Shear-driven failure of liquid-infused surfaces. *Phys. Rev. Lett.* **2015**, *114* (16), 168301.
- (86) Liu, Y.; Wexler, J. S.; Schönecker, C.; Stone, H. A. Effect of viscosity ratio on the shear-driven failure of liquid-infused surfaces. *Phys. Rev. Fluids* **2016**, DOI: 10.1103/PhysRevFluids.1.074003.
- (87) Laney, S. K.; Michalska, M.; Li, T.; Ramirez, F. V.; Portnoi, M.; Oh, J.; Thayne, I. G.; Parkin, I. P.; Tiwari, M. K.; Papakonstantinou, I. Delayed Lubricant Depletion of Slippery Liquid Infused Porous Surfaces Using Precision Nanostructures. *Langmuir* **2021**, *37* (33), 10071–10078.
- (88) Kim, P.; Kreder, M. J.; Alvarenga, J.; Aizenberg, J. Hierarchical or not? Effect of the length scale and hierarchy of the surface roughness on omniphobicity of lubricant-infused substrates. *Nano Lett.* **2013**, *13* (4), 1793–9.

